Contrast-enhanced imaging of cerebral vasculature with laser speckle

K. Murari,* N. Li, A. Rege, X. Jia, A. All, and N. Thakor

Department of Biomedical Engineering, Johns Hopkins University School of Medicine, Baltimore, Maryland 21205, USA

*Corresponding author: kartik@jhu.edu

Received 2 May 2007; accepted 8 May 2007;
posted 30 May 2007 (Doc. ID 82676); published 12 July 2007

High-resolution cerebral vasculature imaging has applications ranging from intraoperative procedures to basic neuroscience research. Laser speckle, with spatial contrast processing, has recently been used to map cerebral blood flow. We present an application of the technique using temporal contrast processing to image cerebral vascular structures with a field of view a few millimeters across and approximately 20 μm resolution through a thinned skull. We validate the images using fluorescent imaging and demonstrate a factor of 2–4 enhancement in contrast-to-noise ratios over reflectance imaging using white or spectrally filtered green light. The contrast enhancement enables the perception of approximately 10%–30% more vascular structures without the introduction of any contrast agent. © 2007 Optical Society of America

OCIS codes: 170.6480, 120.6150.

1. Introduction

The ability to image vascular microstructure is of considerable importance in applications such as clinical diagnostics, basic research, and intraoperative procedures. Conditions such as diabetes and hypertension cause changes in vascular structure before renal and cardiac complications [1,2]. Research areas that require the study of vascular structure, such as angiogenesis, would directly benefit from high-resolution microvascular imaging [3]. In the operating room, the ability to image microvessels would be critical in helping surgeons avoid vascular beds. Current techniques for structural vascular imaging include magnetic resonance imaging (MRI) [4], angiography [5], computed tomography (CT) [6], and vascular casting [7], among others. These techniques lack in spatiotemporal resolution (magnetic resonance, CT, ultrasound) or are invasive procedures involving insertion of catheters or contrast-enhancing agents (angiography, fluorescent imaging). We present a vascular imaging technique based on laser speckle contrast analysis [8] that is minimally invasive and can provide high-contrast images of surface vasculature rapidly without the use of any injected contrast agents. The technique utilizes blood flow as a virtual contrast agent, mapping flows to intensities. Laser speckle imaging has largely been used for creating blood flow maps in tissues like the cortex [9], retinal [10], and skin [11], among others. Recently the technique has also been applied to study changes in blood flow during functional activations such as the electrical somatosensory stimulation of limbs [12], and mechanical whisker stimulation [13] and during neurological insults such as stroke [14] and ischemia [15]. Some work has also been done on the coupling between neural and hemodynamic signals [16], where the technique was used to measure the latter. On the instrumentation aspect, there is recent work on noise reduction schemes [17] and contrast algorithms [18]. Most of this work has been focused toward observing changes in blood flow with high spatiotemporal resolution. However, to our knowledge, the principle of laser speckle contrast has not been applied to structural vascular imaging to study connectivities and morphologies of vascular networks.

In this work we use laser speckle imaging with temporal contrast processing to obtain contrast-enhanced images of the rat cerebral vascular architecture. The images are evaluated and compared with reflectance images obtained in white and spectrally filtered green light using fluorescence imaging as the gold standard. We show increased contrast-to-noise ratios for the speckle images over both white

0003-6935/07/220001-07$15.00/0

and green light images. This increase allows the visualization of structural detail that could not be seen using white or green light. We use a custom setup for acquiring perfectly coregistered images from all three modalities for the comparison.

2. Speckle Contrast and Imaging

Speckle is a random field intensity pattern produced by the mutual interference of partially coherent beams that are subject to minute temporal or spatial fluctuations [19]. These patterns are seen when monochromatic coherent light is incident on a rough surface or a field of scattering particles. If the field of particles is nonstatic, photographing the pattern results in an image that is blurred over the exposure time of the recording device. The velocity information in the blur can be extracted and mapped to contrast using statistical arguments [8,20]. In particular, speckle contrast (K) can be defined as

$$K = \frac{\sqrt{\langle \Delta I^2 \rangle}}{\langle I \rangle}, \tag{1}$$

where the mean, $\langle I \rangle$, and standard deviation, $\sqrt{\langle \Delta I^2 \rangle}$, are calculated along windows slid around the blurred image. Originally K was calculated by considering a window of $N \times N$ pixels that is moved along the image. This results in a spatially contrasted image. Temporal resolution is limited only by the frame rate of the imaging, since each processed image is generated using only one raw laser-illuminated image. However, there is a loss in the spatial contrast by an order of N.

The mean and standard deviation of Eq. (1) can also be calculated over time using a time stack of images [21]. In this case a $1 \times 1 \times M$ pixel window is moved across a time stack of M images to obtain the statistics leading to a temporally contrasted image. This procedure does not lose any spatial resolution but requires several images in time to generate the processed image. The concurrent loss of temporal resolution is acceptable in imaging vascular structure as opposed to functional imaging. For this reason we use temporal contrasting for processing our images.

3. Ground Truth Fluorescent Imaging

The gold standard for vascular architecture imaging is corrosion casting followed by microscopy [7]. However, the procedure requires sacrificing the animal, and comparing the detailed three-dimensional image with two-dimensional nontomographic optical images would be cumbersome. Fluorescent imaging is an accepted technique for obtaining high-quality vascular images [22,23] and was therefore chosen as a benchmark to compare the speckle, white light, and green light images. For this purpose, we obtained coregistered fluorescent, speckle, white, and green light images of the same region of the rat cortex. We used rhodamine-dextran (Invitrogen, Carlsbad, California, USA) as the fluorescent dye. The dye is excited by green light and emits in the red region of the spectrum. Since the fluorophore is conjugated to a large 70,000 molecular weight dextran, it stays within the vessels and does not extravasate, leading to high-quality, high-contrast images of vasculature suitable to evaluate two-dimensional images obtained from the other modalities under comparison.

4. Methods

A. Animal Preparation

All experiments were performed using a protocol approved by the Johns Hopkins Animal Care and Use Committee. Anesthesia was induced in adult female Wistar rats (200–300 g) using a mixture of 4% halothane, 16% oxygen, and 80% nitrous oxide. At the onset of unconsciousness, the rats were anesthetized with a mixture of 43 mg/ml ketamine, 8.6 mg/ml xylaxine, and 1.4 mg/ml acepromazine. Anesthesia was maintained with repeated injections of the same mixture when required. The rat was fixed in a stereotactic frame (David Kopf Instruments, Tujunga, California, USA), and a midline incision was made over the scalp. The temporal muscle was freed and retracted with a No. 4-0 suture line to expose the skull over the barrel cortex. A 5 mm diameter window overlying the barrel cortex, centered at 5.5 mm lateral and 2.5 mm caudal to the bregma, was thinned using a high-speed dental drill (Fine Science Tools, North Vancouver, Canada) equipped with a 1.4 mm steel burr. Saline was used to maintain the temperature during surgery. Thinning was stopped when the inner cortical layer of bone was encountered. The femoral vein of the rat was catheterized and connected to a syringe containing the fluorescent dye.

B. Imaging Setup

The imaging setup consisted of a 12 bit (1280×1024) cooled CCD camera (PCO, Kelheim Germany). The camera was controlled by a dedicated frame grabber card on an image acquisition computer. A 60 mm $f/2.8$ macro lens (Nikon Inc., Melville, New York, USA) with a maximum reproduction ratio of 1:1 at a working distance of 180 mm was mounted on the camera. The lens was mounted using a C mount to a Nikon F mount adapter and had an extension tube to accommodate 1 in. filters (1 in. = 2.54 cm). Thus the maximum reproduction ratio increased to 1.3:1. For fluorescent imaging, a rhodamine emission filter (Chroma, Rockingham, Vermont, USA) could be inserted into the filter tube attaching the lens to the camera. The setup is shown in Fig. 1. The camera was positioned above the prepped animal mounted in the stereotactic frame using a custom-built focusing z drive. The frame was kept on an x–y adjustable stage for precise localization of regions of interest. Three light sources were positioned around the stage. A dc-powered halogen lamp (Pelican, Torrance, California, USA) was used as a white light source. A #58 Wratten (Eastman Kodak, Rochester, New York, USA) gelatin absorption filter was introduced in the light path to illuminate the cortex with spectrally filtered green light. A 0.5 mW, 632.8 nm red HeNe gas laser (JDSU, Milpitas, California, USA) was used

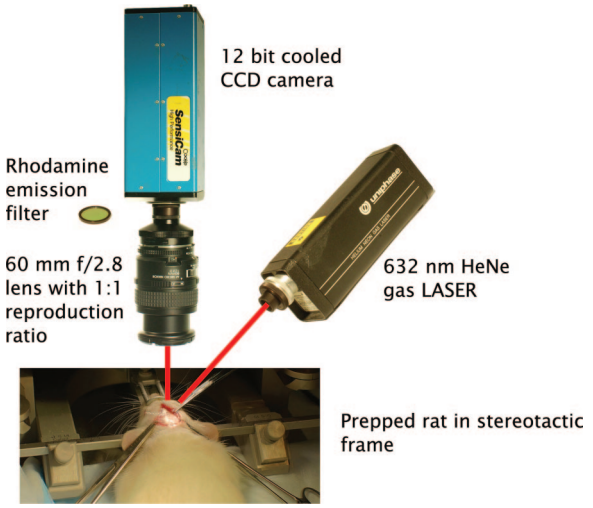

Fig. 1. (Color online) Schematic of the setup used for image acquisition. The rhodamine emission filter is introduced and the laser is switched to green for fluorescent imaging.

for speckle imaging. The initial beam diameter was 0.48 mm and the beam was diverged to cover the region of interest. A 5 mW, 532 nm green diode-pumped solid-state Nd:YVO_4/KTP laser (Beam of Light Technologies, Clackamas, Oregon, USA) laser was used to excite the rhodamine for fluorescent imaging. The excitation was at 532 nm and the emission filter passed a 150 nm band centered around 610 nm.

C. Imaging Protocol

Using the real-time preview from the frame grabber card, the x–y location of the animal and the reproduction ratio on the lens was fixed to obtain the desired field of view. The light sources were adjusted individually to uniformly illuminate the region of interest. Following this, the camera, stage, and all light sources were locked down. To obtain the white light image, the lens was stopped down to $f/16$ to increase the depth of field. A set of 80 images was acquired. Next, the green filter was introduced in the incident light path and another set of 80 images was acquired. For speckle imaging, the aperture of the lens was set according to the lens magnification, laser wavelength, and camera pixel size to optimize the speckle size for contrast calculations [24]. The red laser was turned on and a stack of 80 images was acquired and stored for subsequent processing. To acquire the fluorescent image, the lens was again stopped down to $f/16$ and the rhodamine emission filter was inserted in the optical path. 200 μL of the rhodamine-dextran solution was injected into the bloodstream using the femoral vein catheter. The green laser was switched on and a set of ten images was acquired.

Except for speckle imaging, in all the other cases, the shutter speed was set according to the light intensity and the selected aperture to get a balanced exposure. Since speckle contrast is a flow-based signal, the shutter speed for speckle imaging needs to be chosen with more care than based on the exposure alone. It has been shown that for visualizing smaller vessels a longer exposure time is beneficial [24]. This is due to the lower flow velocities associated with the smaller vessels. This was used along with the aperture stop optimization referred to above to choose an exposure time of 16 ms and an aperture setting of $f/5.6$ for the speckle imaging.

D. Segmentation and Comparison across Modalities

To ascertain the fidelity of the speckle images and a possible improvement over white or green light images, we compared all modalities with fluorescent images, which were taken to be the ground truth. Images from all four modalities were segmented into vessel and background and compared on a pixel-by-pixel basis using the κ coefficient [25]. As described in Subsection 4.C, 80 frames of raw speckle images were processed to generate one contrasted speckle image. To ensure a fair comparison to the white and green light images, 80 frames of the reflectance images were averaged before segmentation. Fewer fluorescent images were used because the $f/16$ aperture setting necessitated exposure times of the order of minutes. Segmentation was carried out by a manual approach with multiple independent observers for increased confidence levels [26]. Ten independent observers were asked to segment images from each modality—white light, green light, speckle, and fluorescent. The ten binary images were then combined into one weighted image with structures being classified as vessels or background with ten confidence levels. The procedure is schematically shown in Fig. 2. Thresholding was applied from five to ten levels leading to binary images ranging from concurrence of five to ten observers on structures being vessels. For each confidence level, the κ coefficient was calculated for the white light, green light, and speckle images as

$$\kappa = \frac{2n(G_{ij} = T_{ij} = 0)}{2n(G_{ij} = T_{ij} = 0) + n(G_{ij} = T_{ij} = 1) + n(G_{ij} = 0; T_{ij} = 1)}, \quad (2)$$

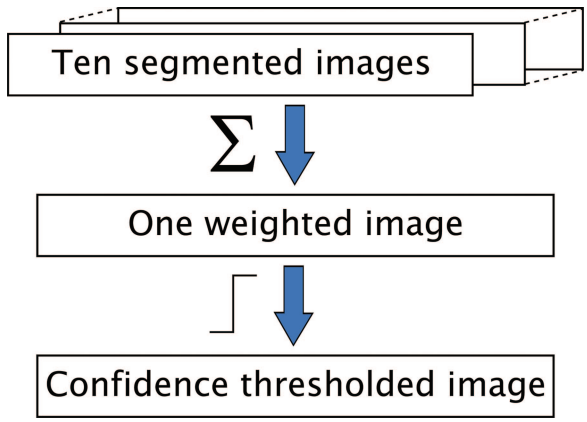

Fig. 2. (Color online) Schematic of the multiobserver manual segmentation procedure used to generate the weighted and confidence thresholded images for comparison.

where the subscripts i and j denote pixel indices and $n(\,)$ denotes the number of pixels satisfying the condition within the parentheses. The test images are denoted by T and the ground truth fluorescent image by G.

E. Contrast-to-Noise Ratio

We take the contrast-to-noise ratio (CNR) definition to be [27]

$$\mathrm{CNR} = \frac{|\mu_{vess} - \mu_{back}|}{\sqrt{f_{vess}\sigma_{vess}^2 + f_{back}\sigma_{back}^2}}, \tag{3}$$

where μ_{vess} and μ_{back} denote the mean intensities of the pixels constituting the vessels and the background, respectively. σ_{vess}^2 and σ_{back}^2 denote the variance in the intensities of the pixels constituting the vessels and the background, respectively. f_{vess} and f_{back} are fractions of the total number of pixels in the image classified as vessel and background, respectively. The numerator is indicative of the intensity difference between vessels and background or the contrast, and the denominator is a measure of the total noise in the image weighted by the composition of the image. Again we use the fluorescent image as the ground truth. Use of the multiobserver weighted white light, green light, and speckle images to segment those modalities would bias the analysis because an observer's perception and segmentation would be effected by the inherent CNR, subsequently effecting the calculated CNR. To perform CNR-independent segmentation, only the weighted fluorescent image was thresholded and segmented. Those segmented areas were then used to extract the vessels and background from all other modalities.

5. Results

Figure 3 shows the white light reflectance, green light reflectance, temporal contrast processed speckle, and fluorescent image of a 6 mm × 7.5 mm area of the rat cortex through a thinned skull. The fluorescent image has been inverted so that vessels appear dark on a lighter background, as is the case with the other two modalities.

Using the procedure outlined in Subsection 4.D, the images shown in Fig. 3 were segmented into vessels and background tissue. The weighted images obtained with ten confidence levels are shown in Fig. 4. To avoid skewing the measurements as a result of artifacts in the periphery of the images, we chose a 512 × 512 pixel region in the center of the images for further analysis. This corresponds to an area of 2.5 mm × 2.5 mm. The confidence levels indicate the number of observers that classify a certain pixel as being part of a vessel and not background tissue. For comparison, the weighted images were thresholded. An image thresholded at $N\%$ meant that at least $N\%$ of the observers concurred on the pixels being segmented as parts of vessels or as parts of background.

To compare fidelity, the fluorescent image was considered as the ground truth, and κ coefficients were calculated for the white light, green light, and speckle

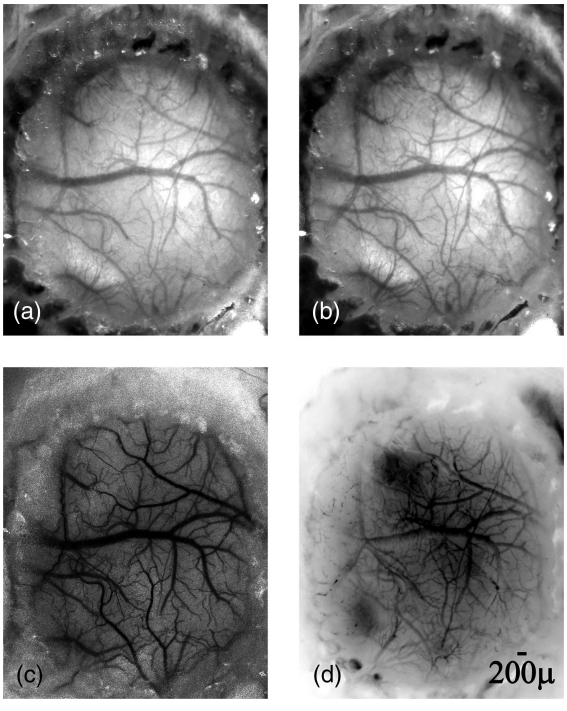

Fig. 3. (a) White light, (b) green light, (c) temporal contrast processed speckle, and (d) fluorescent image of a 6 mm × 7.5 mm area of the rat cortex imaged through a thinned skull. This set of images was used for subsequent comparison and CNR calculations.

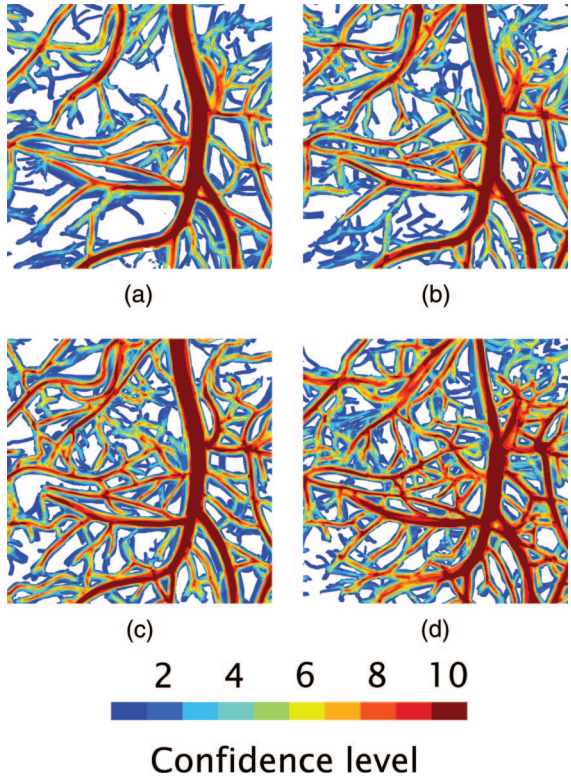

Fig. 4. (Color online) Weighted images with different confidence levels generated from the images shown in Fig. 3.

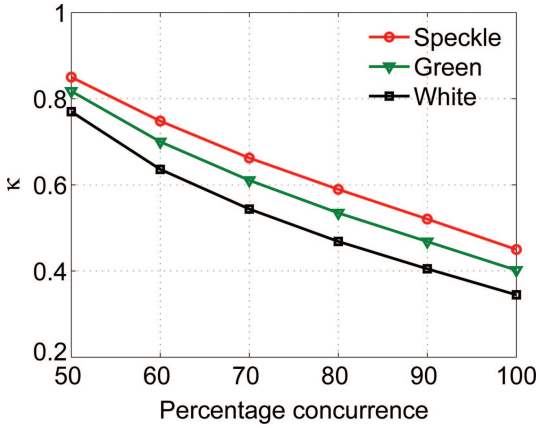

Fig. 5. (Color online) κ coefficient of the speckle, green, and white light images using the fluorescent image as the ground truth. Confidence levels vary on the x axis.

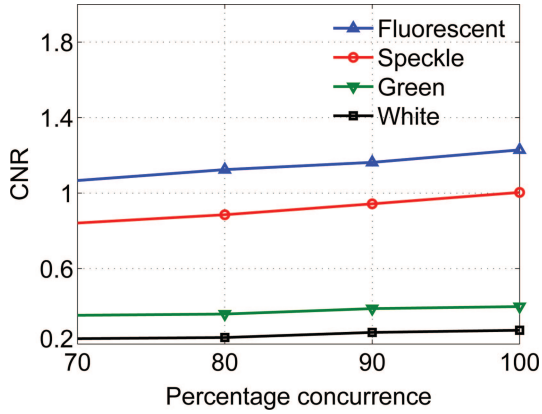

Fig. 7. (Color online) CNRs of images from all modalities calculated after segmentation based on the weighted fluorescent image thresholded at different confidence levels.

images according to Eq. (2) after thresholding the images at confidence levels ranging from 50%–100%. The result is shown in Fig. 5. The higher κ coefficients for the speckle images show that they are closer to the fluorescent images than the white light or the green light images for all thresholds and are therefore a more accurate representation of the vascular architecture.

To compare the CNRs, all images from Fig. 3 were segmented based on our assumed standard—the fluorescent image. The argument for not segmenting each image individually is given in Subsection 4.E. The weighted fluorescent image was thresholded at confidence levels from 70% to 100%. The resulting binary images were used to separate images from all the other modalities into vessels and background. As an example, Fig. 6 shows images from all modalities segmented into vessels and background on the basis of the weighted fluorescent image thresholded at a confidence level of 80%. CNRs were calculated using Eq. (3) and are plotted in Fig. 7. The speckle image can be seen to have a consistently higher CNR, an increase of 3–4 times over the white light and 2–2.5 times over the green light images.

To underscore the ability of this contrast-enhanced imaging technique, we compared the amount of vascular structure that could be perceived through a thinned skull. We compared the relative number of vessels, as seen in Fig. 6, across all modalities. The number of vascular structures and detail that is seen in the speckle image is clearly greater than in the reflectance images. Several structures were missed by the white and green light or had such poor contrast that they had segmentation confidence weights close to zero. Figure 8 shows a quantification of the comparison of vascular structures, the vessel fraction, seen in all modalities for segmentation thresholds from 50%–100%. Vessel fraction is defined as the

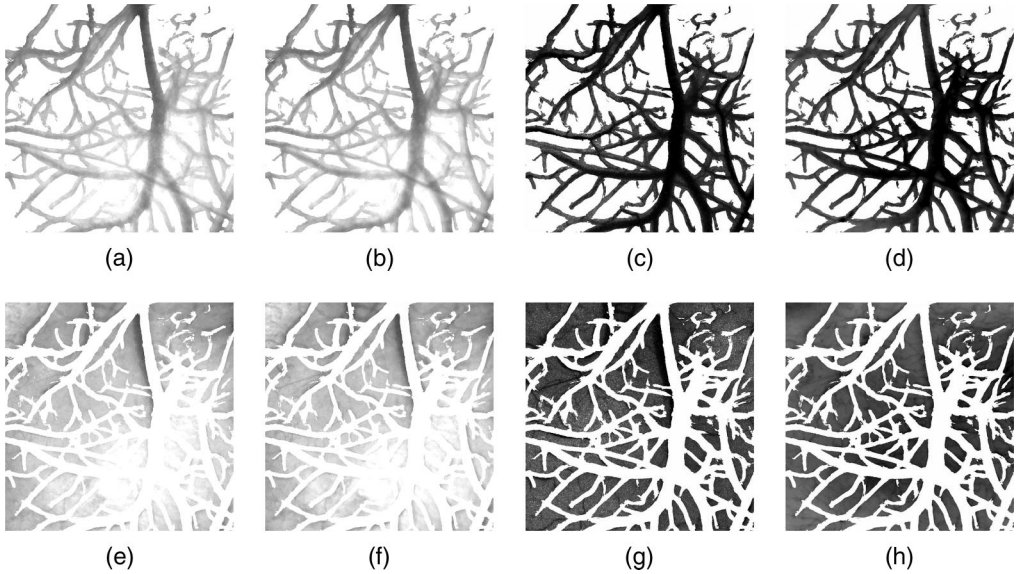

Fig. 6. Images from all modalities segmented into (a)–(d) vessels and (e)–(h) background on the basis of the manually segmented fluorescent image with a confidence threshold of 90%. (a), (e) white light; (b), (f) green light; (c), (g) speckle; and (d), (h) fluorescent.

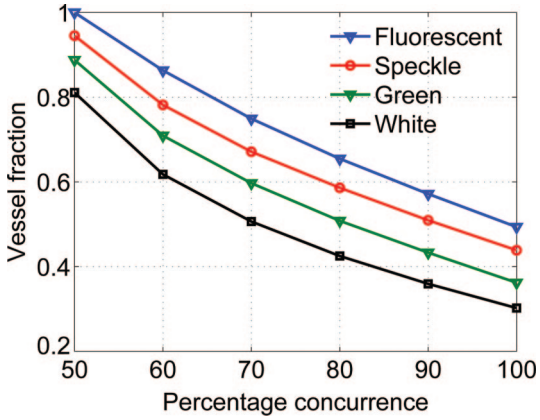

Fig. 8. (Color online) Comparison of the amount of vascular structure contained in the images across all four modalities shown in Fig. 3.

fraction of the pixels present in the image classified as being a part of the vessels after thresholding. All fractions are normalized using the vessel fraction obtained from the fluorescent image at a 50% threshold. The results show that approximately 10%–30% more vascular structures can be seen in the speckle image than in the white or green light reflectance images.

6. Conclusions

We have used the principle of laser speckle combined with temporal contrast processing to image vascular architecture in the rat cortex. Coregistered fluorescent images were used as a standard to compare speckle and reflectance images. Speckle imaging and processing boosts the contrast, without the need for any contrast agent, leading to a twofold to fourfold increase in contrast-to-noise ratios over images obtained in white or spectrally filtered green light. This enhanced contrast enabled the visualization of vascular structures that had too low a contrast to be perceived by reflectance alone. In imaging through a thinned skull, we were able to perceive approximately 10%–30% more structural features using speckle imaging than imaging in white or green light.

The technique is minimally invasive and does not require the introduction of any contrast agents. Thus it does not perturb the vasculature in any way. This makes it more suitable for chronic studies of vascular structure than currently used techniques. It is simple, requiring the use of only a CCD camera and an ordinary laser. Although a two-dimensional surface technique, we believe this will have applications in imaging vascular microarchitecture in superficial tissues such as the retina and the cortical surface.

References

1. N. E. Cameron and M. A. Cotter, "The relationship of vascular changes to metabolic factors in diabetes mellitus and their role in the development of peripheral nerve complications," Diabetes Metab. **10,** 189–224 (1994).
2. F. Hansen-Smith, A. S. Greene, A. W. J. Cowley, and J. H. Lombard, "Structural changes during microvascular rarefaction in chronic hypertension," Hypertension **15,** 922–928 (1990).
3. D. M. McDonald and P. L. Choyke, "Imaging of angiogenesis: from microscope to clinic," Nat. Med. **9,** 713–725 (2003).
4. R. A. Dashner, D. W. Chakeres, A. Kangarlu, P. Schmalbrock, G. A. Christoforidis, and R. M. DePhilip, "MR imaging visualization of the cerebral microvasculature: a comparison of live and postmortem studies at 8 T," Am. J. Neuroradiol. **24,** 1881–1884 (2003).
5. M. Schumacher, "Microangiographic study of the normal anatomy of the cerebral venous system in rats," Neuroradiology **26,** 137–140 (1984).
6. R. von Kummer and J. Weber, "Brain and vascular imaging in acute ischemic stroke: the potential of computed tomography," Neurology **49,** 52–55 (1997).
7. S. H. Aharinejad and A. Lametschwandtner, *Microvascular Corrosion Casting in Scanning Electron Microscopy: Techniques and Applications* (Springer-Verlag, 1992).
8. J. D. Briers and S. Webster, "Laser speckle contrast analysis (LASCA): a nonscanning, full-field technique for monitoring capillary blood flow," J. Biomed. Opt. **1,** 174–179 (1996).
9. A. K. Dunn, H. Bolay, M. A. Moskowitz, and D. A. Boas, "Dynamic imaging of cerebral blood flow using laser speckle," J. Cereb. Blood Flow Metab. **21,** 195–201 (2001).
10. Y. Tamaki, M. Araie, E. Kawamoto, S. Eguchi, and H. Fujii, "Noncontact, two-dimensional measurement of retinal microcirculation using laser speckle phenomenon," Invest. Ophthalmol. Vis. Sci. **35,** 3825–3834 (1994).
11. B. Ruth, "Measuring the steady-state value and the dynamics of the skin blood flow using the non-contact laser speckle method," Med. Eng. Phys. **16,** 105–111 (1994).
12. T. Durduran, M. G. Burnett, G. Yu, C. Zhou, D. Furuya, A. G. Yodh, J. A. Detre, and J. H. Greenberg, "Spatiotemporal quantification of cerebral blood flow during functional activation in rat somatosensory cortex using laser-speckle flowmetry," J. Cereb. Blood Flow Metab. **24,** 518–525 (2004).
13. A. K. Dunn, A. Devor, H. Bolay, M. L. Anderman, M. A. Moskowitz, A. M. Dale, and D. A. Boas, "Simultaneous imaging of total cerebral hemoglobin concentration, oxygenation, and blood flow during functional activation," Opt. Lett. **28,** 28–30 (2003).
14. A. J. Strong, E. L. Bezzina, P. J. B. Anderson, M. G. Boutelle, S. E. Hopwood, and A. K. Dunn, "Evaluation of laser speckle flowmetry for imaging cortical perfusion in experimental stroke studies: quantitation of perfusion and detection of periinfarct depolarizations," J. Cereb. Blood Flow Metab. **26,** 645–653 (2006).
15. A. Ayata, A. K. Dunn, Y. Gursoy-Ozdemir, Z. H. Huang, D. A. Boas, and M. A. Moskowitz, "Laser speckle flowmetry for the study of cerebrovascular physiology in normal and ischemic mouse cortex," J. Cereb. Blood Flow Metab. **24,** 744–755 (2004).
16. A. Devor, A. K. Dunn, M. L. Andermann, I. Ulbert, D. A. Boas, and A. M. Dale, "Coupling of total hemoglobin concentration, oxygenation, and neural activity in rat somatosensory cortex," Neuron **39,** 353–359 (2003).
17. A. C. Volker, P. Zakharov, B. Weber, F. Buck, and F. Scheffold, "Laser speckle imaging with an active noise reduction scheme," Opt. Express **3,** 9782–9787 (2005).
18. P. C. Li, S. L. Ni, L. Zhang, S. Q. Zeng, and Q. M. Luo, "Imaging cerebral blood flow through the intact rat skull with temporal laser speckle imaging," Opt. Lett. **31,** 1824–1826 (2009).
19. J. W. Goodman, "Some fundamental properties of speckle," J. Opt. Soc. Am. **66,** 1145–1150 (1976).
20. J. D. Briers, "Laser Doppler and time-varying speckle: a reconciliation," J. Opt. Soc. Am. A **13,** 345–350 (1996).
21. J. Ohtsubo and T. Asakura, "Velocity measurement of a diffuse

object by using time-varying speckles," Opt. Quantum Electron. **8,** 523–529 (1976).
22. E. J. Yoder and D. Kleinfeld, "Cortical imaging through the intact mouse skull using two-photon excitation laser scanning microscopy," Microsc. Res. Tech. **56,** 304–305 (2002).
23. W. Yu, R. M. Sandoval, and B. A. Molitoris, "Quantitative intravital microscopy using a generalized polarity concept for kidney studies," Am. J. Physiol. Cell. Physiol. **289,** 1197–1208 (2005).
24. S. Yuan, A. Devor, D. A. Boas, and A. K. Dunn, "Determination of optimal exposure time for imaging of blood flow changes with laser speckle contrast imaging," Appl. Opt. **44,** 1823–1830 (2005).
25. J. L. Prince and J. Links, *Medical Imaging Signals and Systems* (Prentice-Hall, 2005).
26. K. H. Fritzsche, A. Can, A. Shen, C.-L. Tsai, J. N. Turner, H. L. Tanenbaum, C. V. Stewart, and B. Roysam, "Automated model based segmentation, tracing and analysis of retinal vasculature from digital fundus images," in *State-of-the-Art Angiography, Applications and Plaque Imaging Using MR, CT, Ultrasound and X-rays,* J. S. Suri and S. Laxminarayan, eds. (Academic, 2003), pp. 225–298.
27. X. M. Song, B. W. Pogue, S. D. Jiang, M. M. Doyley, H. Dehghani, T. D. Tosteson, and K. D. Paulsen, "Automated region detection based on the contrast-to-noise ratio in near-infrared tomography," Appl. Opt. **43,** 1053–1062 (2004).